DRAFT VERSION FEBRUARY 5, 2013
Preprint typeset using LaTeX style emulateapj v. 5/2/11

EFFECTS OF STELLAR ROTATION ON STAR FORMATION RATES AND COMPARISON TO CORE-COLLAPSE SUPERNOVA RATES

SHUNSAKU HORIUCHI[1,2,3], JOHN F. BEACOM[3,4,5], MATT S. BOTHWELL[6,7], TODD A. THOMPSON[4,5]

Draft version February 5, 2013

ABSTRACT

We investigate star formation rate (SFR) calibrations in light of recent developments in the modeling of stellar rotation. Using new non-rotating and rotating stellar tracks of Ekstrom et al. (2012), we study the integrated properties of synthetic stellar populations and find that the UV to SFR calibration for the rotating stellar population is 30% smaller than for the non-rotating stellar population, and 40% smaller for the Hα to SFR calibration. These reductions translate to smaller SFR estimates made from observed UV and Hα luminosities. Using the UV and Hα fluxes of a sample of ~ 300 local galaxies, we derive a total (i.e., sky-coverage corrected) SFR within 11 Mpc of 120–170 $\mathrm{M_\odot\,yr^{-1}}$ and 80–130 $\mathrm{M_\odot\,yr^{-1}}$ for the non-rotating and rotating estimators, respectively. Independently, the number of core-collapse supernovae discovered in the same volume requires a total SFR of $270^{+110}_{-80}\,\mathrm{M_\odot\,yr^{-1}}$, suggesting a mild tension with the SFR estimates made with rotating calibrations. More generally, when compared with the estimated SFR, the local supernova discoveries strongly constrain any physical effects that might increase the energy output of massive stars, including, but not limited to, stellar rotation. The cosmic SFR and cosmic supernova rate data on the other hand show the opposite trend, with the cosmic SFR almost double that inferred from cosmic supernovae, constraining a significant decrease in the energy output of massive stars. Together, these lines of evidence suggest that the true SFR calibration factors cannot be too far from their canonical values.

Subject headings: stars: rotation – stars: formation – supernovae: general

1. INTRODUCTION

The star formation rate (SFR) is one of the principal parameters characterizing galaxies and their evolution. Much effort has been put into deriving SFR indicators from luminosities spanning wavelengths from the radio to the UV (e.g., Kennicutt 1998; Bell 2003; Moustakas et al. 2006; Calzetti et al. 2007; Salim et al. 2007; Kennicutt et al. 2009; Rieke et al. 2009; Calzetti et al. 2010). The efficacy of SFR indicators depends on being able to model the properties of stellar populations at those specific wavelengths. The modeling is typically condensed into "calibration factors" that are the ratios of the SFR and the luminosity in a given band, for a given assumed underlying stellar population. For example, the SFR estimated using the Hα indicator is the observed Hα luminosity, appropriately dust-corrected, multiplied by the Hα calibration factor.

Calculating the calibration factors for the various SFR indicators requires a great deal of complex physics, including challenging problems such as the evolution of massive stars and its dependence on stellar parameters such as mass, metallicity, and rotation; stellar atmospheres; the binary fraction and the resulting interactions; the shape of the stellar initial mass function (IMF); whether star formation is continuous or variable; and so on. The status was summarized by Kennicutt (1998), who indicated a spread of ~ 0.1 dex in Hα calibration factors (~ 0.3 dex in the UV) in the literature when compared for common assumptions of metallicity and IMF[8]. These uncertainties have typically been subdominant compared to the far larger spread between SFR measurements made by different surveys and indicators. However, the global SFR density and its redshift evolution have been increasingly well mapped in recent years (e.g., Lilly et al. 1996; Madau et al. 1996, 1998; Steidel et al. 1999; Hopkins 2004). The spread between different SFR density measurements at low redshifts $0 < z < 1$ is now only several tens of percent (Hopkins & Beacom 2006, hereafter HB06)[9], motivating a renewed look at the calibration uncertainties.

One of the potentially very important physical inputs not considered in many early calibration studies is stellar rotation. Although the standard non-rotating theories of stellar evolution have been highly successful, new data lead to a number of serious discrepancies, and the quantitative effects of rotation have been significantly advanced in the past decade (see,

[1] s.horiuchi@uci.edu
[2] Center for Cosmology, University of California Irvine, 4129 Frederick Reines Hall, University of California, Irvine, CA 92697 URL: http://www.physics.uci.edu/
[3] Center for Cosmology and Astro-Particle Physics, The Ohio State University, 191 West Woodruff Ave., Columbus, OH 43210 URL: http://ccapp.osu.edu/
[4] Department of Physics, The Ohio State University, 191 W. Woodruff Ave., Columbus, OH 43210 URL: http://www.physics.ohio-state.edu/
[5] Department of Astronomy, The Ohio State University, 140 West 18th Ave., Columbus, OH 43210 URL: http://www.astronomy.ohio-state.edu/
[6] Steward Observatory, University of Arizona, Tucson, AZ 85721, USA URL: http://www.as.arizona.edu/
[7] Cavendish Laboratory, University of Cambridge, 19 J.J. Thomson Avenue, Cambridge, CB3 0HE, UK URL: http://www.phy.cam.ac.uk/

[8] Reasonable variations of the IMF introduce an overall uncertainty of a factor of ~ 2. However, we will test the SFR using supernovae in a way that is weakly affected by changes to the IMF; see Section 4.

[9] HB06 also assumes a common metallicity and IMF, and notes that IMF variations dominantly affect the accuracy (normalization) instead of the precision (scatter), as long as the IMF variations are universal.

e.g., reviews by Maeder & Meynet 2000; Langer 2012). Importantly, stellar rotation impacts stellar evolution through its effect on stellar mixing and mass loss (e.g., Meynet & Maeder 2000; Heger & Langer 2000; Brott et al. 2011). This affects the massive O and B stars that drive the determination of the SFR calibration factors.

Recently, Ekström et al. (2012) presented evolutionary tracks of single stars at solar metallicity, including a complete grid of tracks that have a detailed treatment of axial rotation (the "ROT" tracks, to distinguish from the non-rotating "NOROT" tracks). In the ROT tracks, they assume initial rotations of $v_{\rm ini} = 0.4 v_{\rm crit}$, where $v_{\rm crit}$ is the velocity where the centrifugal and gravitational accelerations are equal, and the ratio of 0.4 is motivated by the peak of the velocity distribution observed in young B stars (Huang et al. 2010).

If rotation at the level assumed in the ROT tracks of Ekström et al. (2012) is ubiquitous among stars, it implies a number of changes and improvements over the NOROT tracks. For example, they provide a better description of the observed properties of Wolf-Rayet stars, including the Wolf-Rayet type ratios, as well as the resulting core-collapse supernova (CCSN) type ratios (Georgy et al. 2012). They also show considerably improved agreement with the positions of evolved yellow and red supergiants on the HR diagram, as observed in M 33 (Drout et al. 2012) and the Large Magellanic Cloud (Neugent et al. 2012). Similarly, it has been shown that the increased mass loss rates result in better agreement with the observed yellow supergiant CCSN progenitors (Georgy 2012). Furthermore, using the Starburst99 (Leitherer et al. 1999) evolutionary synthesis code, Levesque et al. (2012) has shown that the ionizing radiation field produced by a population of ROT stars is considerably harder than those produced by a population of NOROT stars. The difference reaches an order of magnitude in the ionizing $\lambda < 228$ Å flux. They also note that the bolometric luminosity of the ROT population is higher by a factor ~ 2 for the first ~ 10 Myr.

Such changes to the photon output of stellar populations will impact SFR measurements that are derived from observed galaxy luminosities. We quantitatively assess whether these proposed changes are consistent with observations of star formation and CCSN rates.

We quantify for the first time the effects of stellar rotation as modeled by Ekström et al. (2012) on SFR calibration factors. Previously, Leitherer (2008) used the rotational stellar tracks of Meynet & Maeder (2000) and reported $\sim 25\%$ reductions in SFR calibration factors. We base our calculations on the newer ROT tracks of Ekström et al. (2012) and find larger effects.

We then quantitatively investigate whether the new SFR calibrations are consistent with recent SFR and CCSN data. Since CCSNe mark the ends of the most massive stars formed in a star formation burst, their occurrence is an excellent proxy for recent star formation. CCSNe are particularly suited for our purposes of testing the effects of the ROT tracks on SFR calibrations, because CCSNe provide a benchmark SFR that is minimally affected by stellar rotation: in other words, while stellar rotation is a major parameter affecting what *type* of CCSN a collapsing star becomes, the total *number* of CCSNe, when all Types II and Ibc are included, likely remains only weakly affected. In addition, the SFR-CCSN comparison is only weakly dependent on the IMF, which allows us to avoid the large uncertainty introduced by IMF variations.

We focus on both the cosmic and more local distance regimes. For the latter, we make new calculations of the SFR in the nearby Universe within 11 Mpc (we henceforth refer this volume simply as the "local volume"), update the discovery list of local CCSNe, and perform a comparison of the two. The local volume provides a unique test that is complementary to comparisons at cosmic distances, since it is dependent on different inputs with different systematic effects. The completeness of CCSN searches has also improved in recent years, enabling a meaningful analysis with decent statistics. For example, CCSNe in the local volume have been recently utilized in the study of dim CCSNe (Horiuchi et al. 2011), the mass range of CCSNe (Botticella et al. 2012), and strongly dust-obscured CCSNe (Mattila et al. 2012). Here, we use it to study the SFR calibration factors.

The paper is organized as follows. In Section 2, population synthesis results are presented and the SFR calibration factors are calculated. In Section 3, the effects on SFR measurements are discussed, for both the cosmic and local distances. We then study the comparison with observed CCSN rates in Section 4. We finish with discussion and a summary in Section 5. Throughout, we adopt the standard ΛCDM cosmology with $\Omega_m = 0.3$, $\Omega_\Lambda = 0.7$, and $H_0 = 70$ km s^{-1} Mpc^{-1}.

2. EFFECTS OF NEW STELLAR TRACKS ON SFR ESTIMATORS

2.1. *Integrated properties of stellar populations*

We use the PEGASE.2 evolutionary synthesis code (Fioc & Rocca-Volmerange 1999) to investigate integrated properties of synthetic stellar populations. The default tracks come mainly from the Padova group (Alongi et al. 1993; Bressan et al. 1993; Fagotto et al. 1994a,b,c; Girardi et al. 1996, henceforth "Padova96"). These are non-rotational stellar tracks covering a wide range of mass and metallicities. To obtain a complete set of stellar evolutionary tracks, PEGASE.2 combines AGB, white dwarf, and unevolving stellar evolutions by various authors (Groenewegen & de Jong 1993; Althaus & Benvenuto 1997; Chabrier & Baraffe 1997). Throughout, we adopt a fixed metallicity of $Z = 0.014$ in order to match the metallicity of the tracks by Ekström et al. (2012). Furthermore, we adopt the supernova model B of Woosley & Weaver (1995), a close binary fraction of 0.05, no galactic winds, no treatment of dust extinction, and a minimum core-collapse supernova mass of $8 M_\odot$. In PEGASE.2, the supernova model and the minimum mass are only used for calculations of metal enrichment. We checked that changing these parameters do not change the integrated population emission properties noticeably. Unless otherwise stated, we adopt a Salpeter IMF with slope $dN/dM \propto M^\alpha$ with $\alpha = -2.35$ over the mass range 0.1–$100 M_\odot$ (Salpeter 1955).

The NOROT and ROT tracks of Ekström et al. (2012) are for fixed metallicity ($Z = 0.014$) and extend to the core He-flash, early-AGB, and the end of the core C burning for low, intermediate, and massive stars, respectively. Since we are interested in the first ~ 100 Myr of evolution and in bands

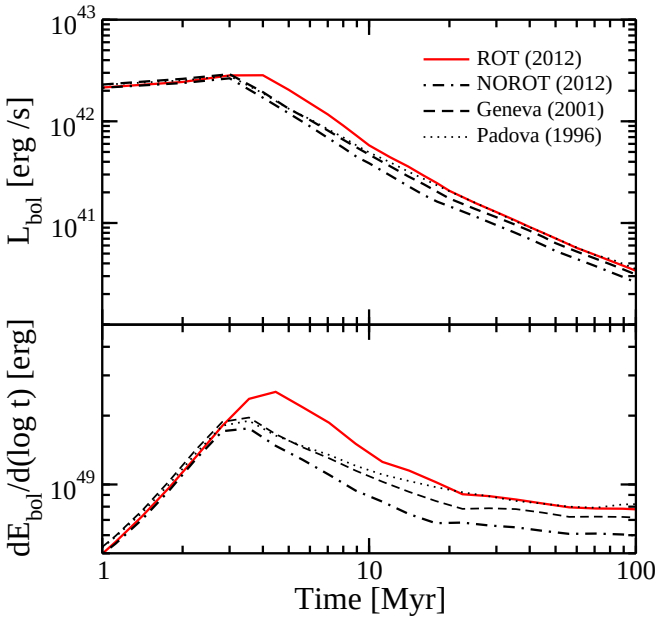

FIG. 1.— Top panel: bolometric luminosity ($dE_{\rm bol}/dt = L_{\rm bol}$) following a burst of star formation with a fixed stellar mass of $10^6 M_\odot$, for the stellar tracks of Padova96 (non-rotating; dotted), Geneva01 (non-rotating; dashed), and for Ekström et al. (2012): NOROT (non-rotating, dot-dashed) and ROT (rotating, red solid). Bottom panel: the luminosity per logarithmic time bin ($dE_{\rm bol}/d\log t$), illustrating the nearly constant energy output after reaching a peak at $\sim$ 4 Myr when the most massive stars begin to disappear due to core collapse.

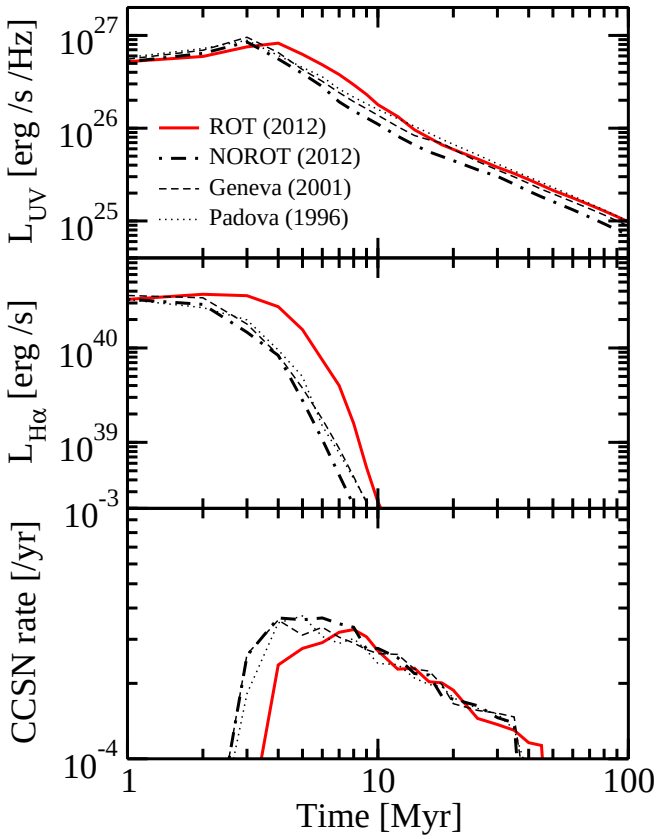

FIG. 2.— Quantities following a burst of star formation: UV (0.2μm) luminosity (top panel), Hα luminosity (middle panel), and the CCSN rate (bottom panel). Star formation burst properties are same as in Figure 1. The UV luminosity evolves similarly to the bolometric luminosity, since a wide range of stars ($\sim$ 3–20$M_\odot$) contribute to the UV band. On the other hand, the Hα luminosity is powered by the most massive stars ($\gtrsim 20 M_\odot$) and its behavior is qualitatively different.

where massive stars dominate, these tracks are generally sufficient. For example, the central evolution of massive stars beyond C-burning is usually short enough that the surface properties are no longer modified, and we also do not need to include white dwarf tracks. We adopt the same supernova, dust, binary, and IMF assumptions as described above for the Padova96 population. For comparison purposes, we also consider the non-rotating tracks by Schaller et al. (1992) and Lejeune & Schaerer (2001), henceforth "Geneva01".

We first simulate an instantaneous burst of star formation with a fixed stellar mass of $10^6 M_\odot$ and follow the evolution of this stellar population up to 100 Myr. Such a coeval stellar population can be used for studying different stellar samples as the population ages. Figure 1 shows the resulting bolometric luminosity. We confirm previous works (e.g., Leitherer & Ekstrom 2011; Levesque et al. 2012) and find that the ROT population is 0.4–0.5 mag more luminous than the NOROT population. This difference is a consequence of rotation-induced mixing. This allows stars to burn more hydrogen and increase the main sequence lifetimes by about 25%. They also have higher luminosities than the NOROT stars. These echo the results of Brott et al. (2011) who also show luminosities and temperatures increase for fast rotation. We continue to observe this difference out to 100 Myr, which is consistent with the fact that the rotational effects are observed for all stars above $\sim 2 M_\odot$ (Ekström et al. 2012). In the bottom panel we show how the energy output appears in bins of logarithmic time.

The NOROT population evolves similarly to those based on the older non-rotating tracks of Padova96 and Geneva01, but after several Myr becomes slightly underluminous. This is due to the updated overshooting and mass-loss prescriptions of the NOROT tracks. These decrease the main sequence lifetime of $M < 30 M_\odot$ mass stars and increases the main sequence lifetime of $M > 30 M_\odot$ stars, respectively (see Figure 6 of Ekström et al. 2012). Therefore, after a few Myr when the most massive stars have exploded, the difference between populations are dominated by $M < 30 M_\odot$ stars, and the NOROT population is expected to become dimmer compared to the Padova96 and Geneva01 populations. However, the differences are small, and we will henceforth quote effects of rotation relative to the updated non-rotational NOROT tracks unless specifically stated otherwise.

In Figure 2, we show the UV (0.2μm) luminosity, the Hα luminosity, and the CCSN rate following the same star formation burst. The UV luminosity evolution is similar to that of the bolometric luminosity, because the dominant contribution comes from a wide mass range of stars; for our adopted tracks, $\sim$ 3–20$M_\odot$ stars. On the other hand, the Hα luminosity shows a qualitatively different behavior. This is because the Hα emission is largely sensitive to photons shortward of the Lyman limit that dominantly arise from massive young stars with $M \gtrsim 20 M_\odot$. The Hα thus falls when these massive stars disappear in core collapse. The progenitors of CCSN are $M > 8 M_\odot$ stars that fall in between the UV and Hα in terms of mass range. Thus it rises when the most massive $100 M_\odot$

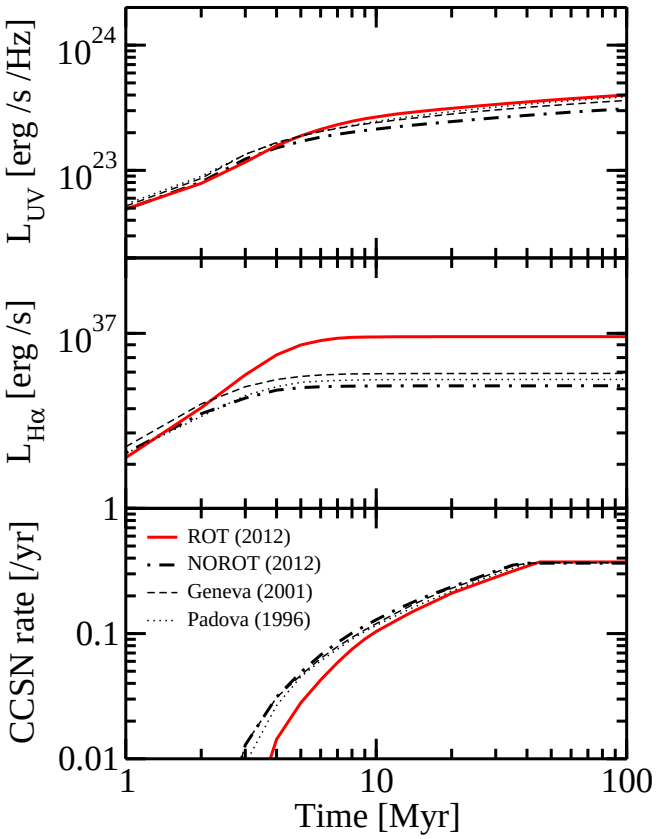

FIG. 3.— Same as Figure 2 but for a continuous star formation rate of $50\,\mathrm{M_\odot\ yr^{-1}}$. The H$\alpha$ reaches equilibrium earliest since they are sourced by the most massive stars only. The progenitors of CCSNe are $M > 8M_\odot$ stars that reach equilibrium later, while the UV has some contribution from stars with lifetimes longer than 100 Myr.

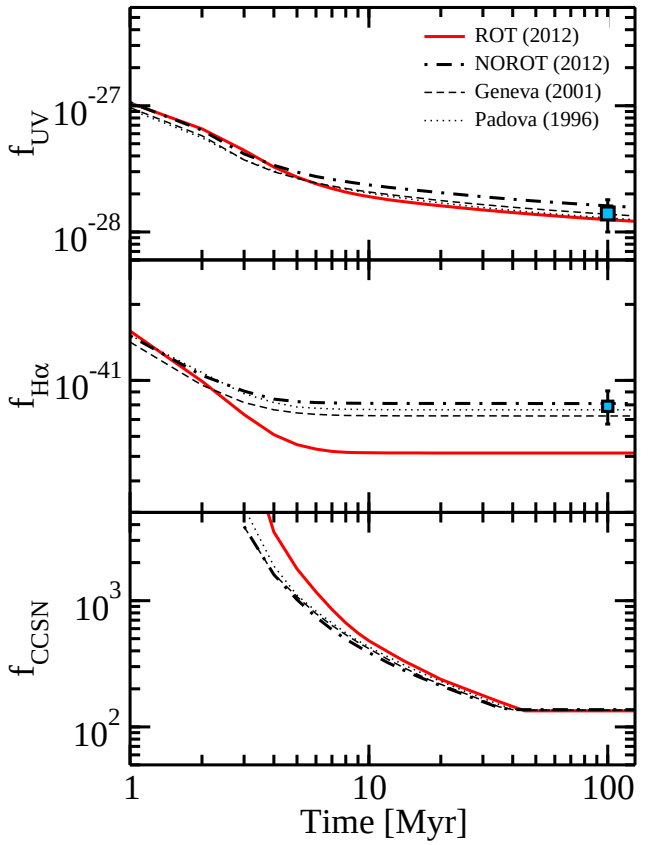

FIG. 4.— UV (top panel) and Hα (middle panel) calibration factors calculated under the continuous star formation approximation starting at time $t = 0$. Calibration factors are defined such that $\mathrm{SFR} = f_x L_x$, i.e., in units of $(M_\odot \mathrm{yr}^{-1})/(\mathrm{erg\,s^{-1}\,Hz^{-1}})$ and $(M_\odot\,\mathrm{yr}^{-1})/(\mathrm{erg\,s^{-1}})$ for the UV and Hα, respectively. For comparison, we mark the values quoted in Kennicutt (1998) as a data point. In the bottom panel we show the CCSN calibration factor (see Section 4 for details).

stars core collapse and falls when the least massive $8M_\odot$ stars undergo core collapse. For the CCSN rate, the difference between tracks is only due to the different main sequence lifetimes of the CCSN progenitors. For example, the ROT tracks with their longer main sequence lifetimes shows a later rise in the CCSN rate. On the other hand, the UV and Hα properties also strongly reflect the differences in luminosity and surface temperature.

2.2. *Star formation rate calibration factors*

A variety of indicators are used as tracers of recent star formation activity, all directly or indirectly probing the current population of massive stars (e.g., Kennicutt 1998; Bell 2003; Moustakas et al. 2006; Calzetti et al. 2007; Salim et al. 2007; Kennicutt et al. 2009; Rieke et al. 2009; Calzetti et al. 2010). The UV stellar continuum and the Hα nebular emission have traditionally been extensively used due to their accessibility. We compute the UV and Hα calibration factors using PEGASE.2 assuming standard assumptions of constant star formation rate for at least 100 Myr. This is the continuous star formation approximation, which provides enough time to allow the birth and death of massive stars that dominate the luminosity in the UV and Hα to equilibrate. It is applicable at least at low-z where the fraction of the total SFR contributed from young starbursts is thought to be $< 10\%$ (e.g., Salim et al. 2005).

In Figure 3, we show the UV (0.2μm) luminosity, the Hα luminosity, and the CCSN rate, all for a continuous star formation rate of $50\,\mathrm{M_\odot\ yr^{-1}}$. As can be seen, the H$\alpha$ luminosity and CCSN rate comfortably reach equilibrium before 100 Myr. By contrast, the UV is still marginally increasing because the UV has contributions from stars with main sequence lifetimes longer than 100 Myr. However, this is not a large fraction. The UV luminosity only increases by another $\sim 15\%$ over the next few hundred Myrs before reaching equilibrium. It should be mentioned that the CCSN rate for different stellar tracks all tend to the same value. This is because we have defined the CCSN rate by the mass range of stars undergoing core collapse (see Section 4 for more details).

We define the calibration factor f_x by

$$\mathrm{SFR} = f_x L_x, \tag{1}$$

where SFR is in units $M_\odot\,\mathrm{yr}^{-1}$, and L_x is the dust-corrected luminosity in units $\mathrm{erg\,s^{-1}}$ for the Hα and $\mathrm{erg\,s^{-1}\,Hz^{-1}}$ for the UV. Results for the Padova96, Geneva01, NOROT, and ROT tracks are shown in Figure 4 where their time evolution are shown, and their values for 100 Myr after the onset of star formation are summarized in Table 1. Firstly, we see that the new NOROT calibrations are similar to the Padova96, Geneva01, and Kennicutt (1998) calibrations, although they

TABLE 1
SUMMARY OF $Z = 0.014$ CALIBRATION FACTORS FOR SALPETER IMF AT 100 MYR (CONTINOUS SFR)

	$f_{\rm UV}$	$f_{\rm H\alpha}$
Kennicutt (1998)	1.4×10^{-28}	7.9×10^{-42}
Padova (1996)	1.3×10^{-28}	7.7×10^{-42}
Geneva (2001)	1.4×10^{-28}	7.2×10^{-42}
NOROT (2012)	1.6×10^{-28}	8.1×10^{-42}
ROT (2012)	1.2×10^{-28}	5.2×10^{-42}

NOTE. — Calibrations defined as $f_x = {\rm SFR}/L_x$. The Hα calibration has units of $(M_\odot\ {\rm yr}^{-1})/({\rm erg\,s}^{-1})$ and the UV calibration has units of $(M_\odot {\rm yr}^{-1})/({\rm erg\,s}^{-1}\,{\rm Hz}^{-1})$.

are slightly larger. For example, compared to the commonly used values of Kennicutt (1998), the UV calibration is larger by $\sim 10\%$. Secondly, the ROT tracks yield smaller calibrations. For example, the ROT UV and Hα calibrations are smaller by 30% and 40% when compared to the NOROT calibrations. These follow from the increased main sequence lifetimes and luminosities of rotating stars. The widely adopted calibrations of Kennicutt (1998) are shown for comparison with error bars that reflect the full range of values reported by Kennicutt (1998). Most of our calibrations from Table 1 are within this range, but the ROT Hα calibration is significantly lower.

We change the PEGASE.2 input parameters to test the robustness of these results. One of the most important inputs for calculating the calibration factor is the IMF. Generally, a shallower (steeper) IMF results in relatively more (less) massive stars and smaller (larger) calibration factors. We consider three IMFs for comparison: the "SalA" IMF, as proposed by Baldry & Glazebrook (2003), with the Salpeter shape above $0.5M_\odot$ (high-mass gradient of -2.35) and a suppression below $0.5M_\odot$ (low-mass gradient of -1.5); the "BG" IMF, also by Baldry & Glazebrook (2003), with a high-mass gradient of -2.15 and a low-mass gradient of -1.5; and finally, the IMF of Kroupa (2001). The SalA, BG, and Kroupa IMFs respectively yield UV calibration factors that are ~ 0.77, ~ 0.50, and ~ 0.83 times those of the Salpeter IMF, all for the NOROT tracks. The Hα changes slightly more: by ~ 0.77, ~ 0.42, and ~ 0.79, respectively.

Repeating the exercise with the ROT tracks, very similar changes are observed. For example, the SalA, BG, and Kroupa IMFs yield UV calibration factors that are ~ 0.78, ~ 0.49, and ~ 0.83 times those of the Salpeter IMF, and Hα calibration factors that are ~ 0.77, ~ 0.41, and ~ 0.79 times those of the Salpeter IMF. Therefore, while the absolute values of the calibrations change as a result of the IMF shape, the relative importance of stellar rotation is always a reduction of 30–40%. We also stress here that the IMF does not strongly impact the comparison with the CCSN rate (see Section 4).

Changing the mass range of the IMF also makes a difference to the SFR calibrations. For example, increasing the high-mass cutoff from our canonical $100M_\odot$ to $120M_\odot$ leads to more massive stars (for a fixed total stellar mass) and a 3% and 15% decrease in the UV and Hα NOROT calibrations, respectively. Some authors adopt an upper limit of $60M_\odot$ which would have the opposite effect: 12% and 60% increases, respectively. We note here that the use of $60M_\odot$ necessarily underestimates the Hα calibration because the important massive stars are not included. Once again, the effect of rotation is a 30–40% reduction in the calibration factors regardless of the mass range. This is partly due to the assumption of a rotation velocity $v_{\rm ini} = 0.4v_{\rm crit}$ for all stellar masses of the ROT tracks.

Metallicity is also important since the evolution of massive stars are strongly affected by metal-driven mass loss (e.g., Kudritzki et al. 1989). Generally, low-metallicity stars are larger and more luminous, leading to smaller SFR calibration factors. For the Padova96 tracks and a Salpeter IMF, changing the metallicity to $Z = 0.001$ ($Z = 0.1$) causes the UV calibration to change by -2% ($+10\%$) when compared to our canonical $Z = 0.014$ estimates, and the Hα calibration to change by -30% ($+50\%$). We do not quantitatively study rotation effects for different metallicities since the Ekström et al. (2012) tracks are only for a single metallicity. However, rotation effects are less important for high-metallicity stars whose evolutions are more strongly affected by metal-driven mass loss (Brott et al. 2011). Other parameters such as the minimum mass for CCSNe, the supernova chemical abundance model, and the presence of Galactic winds, only slowly affect the luminous outputs of stars through feedback of chemically enriched gas.

Other star formation indicators that are routinely used include the [OII]$\lambda 3727$ forbidden line, infrared, and radio emissions. We do not calculate calibrations for these directly. However, because they are often associated with either the UV or Hα, we can discuss how they are affected by stellar rotation. For example, the [OII] luminosity is not directly coupled to the ionizing luminosity, but as a SFR tracer it is empirically calibrated based on Hα, often using samples of nearby galaxies (Kennicutt 1992; Moustakas et al. 2006). This is nontrivial since the [OII] to Hα ratio depends on the luminosity, metallicity, and also obscuration. But it implies that changes to the Hα calibration factor will be carried through to a change in the [OII] calibration factor.

The infrared luminosity is an indirect tracer of star formation arising from UV continuum that is absorbed and reradiated by dust. It is complementary to the UV and Hα that that are absorbed by dust, and calibrations have been investigated by many authors (Sauvage & Thuan 1992; Bell 2003; Calzetti et al. 2007; Rieke et al. 2009; Calzetti et al. 2010). It requires sufficient optical depth of the dust in the star formation region, such that the $L_{\rm IR}$ provides a calorimetric measure of the star formation. However, in practice, the infrared is contaminated by dust heated by old stellar populations. For spiral galaxies the contamination to the far-infrared (1–1000μm) can be as high as 70% (e.g., Lonsdale & Helou 1987), and modern calibrations therefore utilize shorter wavelengths where contamination is less of an issue (Calzetti et al. 2010). So, rotation effects on the low-mass stellar population must also be considered to some degree, depending on the galaxy sample and exact wavelength used. According to Ekström et al. (2012), rotation affects low mass stars (0.8–

$2M_\odot$) less than the massive stars, which means that the infrared calibrations will be less affected by stellar rotation than the UV or Hα.

Radio continuum emission is another indirect tracer of star formation. It is insensitive to dust attenuation, but it relies on the complex and poorly understood physics of cosmic ray production and confinement in supernova remnants. The 1.4 GHz SFR calibration of Bell (2003) partly avoids this difficulty by empirically using the observed tight radio-FIR correlation, and calibrating to be consistent with the FIR calibration of Kennicutt (1998). This calibration is a factor ~ 2 smaller than the calibration of Condon (1992) that is calculated from first principles. Rotation will reduce the radio calibrations of Bell (2003) through the infrared calibration, but will not affect those of Condon (1992).

To conclude, recent modeling of stellar rotation imply reductions in SFR calibration factors by 30% for the UV and 40% for the Hα, where we have compared the ROT population to the NOROT population. Comparing the ROT calibrations to the widely-used non-rotating calibrations of Kennicutt (1998), the reductions are 10% and 40% for the UV and Hα, respectively.

3. IMPLICATIONS FOR SFR ESTIMATES

The reductions to the SFR calibration factors due to stellar rotation are somewhat smaller than the reductions caused by variations in the IMF (~ 0.77 for SalA and ~ 0.50 for BG). Nevertheless, they have testable consequences. As we discuss in Section 4, observations of CCSNe provide a benchmark SFR whose comparison with the directly measured SFR is minimally dependent on the IMF. Also, because stellar rotation affects the Hα indicator more than the UV, we can use the UV/Hα ratio as a test.

3.1. *SFR at cosmic distances*

At cosmic distances, the SFR has been measured by many groups using a variety of indicators. Comparisons of data are complicated by different galaxy selection biases, different assumptions of dust attenuation, different luminosity cuts, cosmic variance, and other issues (e.g., Hopkins et al. 2001; Hopkins 2004). To address these, HB06 selected recent SFR data, converted them to a common cosmology, dust correction scheme, IMF, and calibration assumptions. Using their compilation, they found a best-fit cosmic SFR density with a $z = 0$ normalization of $2.0^{+0.4}_{-0.3} \times 10^{-2}\,\mathrm{M_\odot\,Mpc^{-3}\,yr^{-1}}$ (1σ errors) for a Salpeter IMF and SFR calibrations of Kennicutt (1998).

The HB06 best-fit uncertainty is $\pm$20–30% in the most constrained redshift range of $0 < z < 1$. In this redshift range, the HB06 fit is based mostly on UV-derived SFR measurements, except for one Hα measurement at $z \approx 0.01$ by Hanish et al. (2006). Changing the UV calibration from their adopted Kennicutt (1998) values to our ROT values only results in a mild $\sim 10\%$ reduction in the SFR, which is smaller than the fit uncertainty. At larger redshifts, a wider range of indicators are used in the HB06 fit. Since stellar rotation affects different indicators by different degrees, stellar rotation will contribute additional spread as well as reduce the SFR normalization. However, the HB06 best-fit uncertainty is factors of ~ 2 or more at these larger redshifts, so rotation would not be a dominant contributor to the uncertainty.

3.2. *SFR at local distances*

In contrast to the cosmic SFR, studies of the local volume within ~ 10 Mpc have the advantage that all use almost identical galaxy samples. The 11 Mpc Hα and Ultraviolet Galaxy Survey (11HUGS) is designed to provide a census of the SFR in the volume within 11 Mpc using the Hα indicator (Kennicutt et al. 2008). The distance limit was set to have both statistically significant galaxy numbers (436 galaxies) and galaxy completeness ($M_B = -15$ mag at the distance limit 11 Mpc; however, the number of galaxies as a function of distance does not rise as fast as expected from a constant density of galaxies, as shown in Figure 5). These local galaxies have also been observed by the $GALEX$ and $Spitzer$ satellites, providing multi-band UV and IR photometry: these are the GALEX Nearby Galaxy Survey (390 galaxies, including 363 from the 11HUGS; Gil de Paz et al. 2007; Lee et al. 2011) and the composite Local Volume Legacy survey (LVL, with a total of 258 galaxies, including 231 from the 11HUGS; Dale et al. 2009).

Using a sample of ~ 300 local galaxies, Lee et al. (2009) carefully investigated the Hα- and UV-SFR. After correcting for dust, they find that the Hα-SFR tend to be smaller than the UV-SFR, $\log(\mathrm{SFR_{UV}}/\mathrm{SFR_{H\alpha}}) \approx 0.13$, i.e., a factor of 1.35, for the most star-forming galaxies with Hα-SFR $> 10^{-1.5}\,\mathrm{M_\odot yr^{-1}}$. In another study, Botticella et al. (2012) studied 312 local galaxies and derived dust-corrected Hα and UV luminosities of $L_{\mathrm{H}\alpha} = (99 \pm 5) \times 10^{41}\,\mathrm{erg\,s^{-1}}$ and $L_{\mathrm{UV}} = (88 \pm 6) \times 10^{28}\,\mathrm{erg\,s^{-1}\,Hz^{-1}}$, respectively. Using the calibrations of Kennicutt (1998), they find Hα- and UV-SFR values of $78 \pm 4\,\mathrm{M_\odot yr^{-1}}$ and $123 \pm 8\,\mathrm{M_\odot yr^{-1}}$, respectively.

If we apply the ROT calibration factors to the local luminosities of Botticella et al. (2012), the difference between the Hα- and UV-SFR will widen from their nominal ratio of UV-SFR/Hα-SFR ≈ 1.6 to UV-SFR/Hα-SFR > 2. This difference is considerably larger than thes reported measurement errors, and disfavors ubiquitous stellar rotation in the local galaxies. However, it is premature to conclude that stellar rotation is not allowed by local SFR estimates. On an individual galaxy basis, different indicators give discrepant SFR estimates, sometimes up to factors of ~ 10 (Hopkins et al. 2003). Although the difference is much reduced for larger samples of galaxies, systematic uncertainties in flux measurements, dust attenuation corrections, stochasticity in the formation of high mass stars, variations in the IMF, and departures from standard recombination calculations can still result in systematic offsets between the two indicators (e.g. Buat et al. 1987; Buat 1992; Hopkins et al. 2001; Buat et al. 2002; Bell & Kennicutt 2001; Iglesias-Páramo et al. 2004; Salim et al. 2007; Bothwell et al. 2009). Of these, the most plausible source of problems is dust corrections. Indeed, Botticella et al. (2012) argues the UV-Hα discrepancy arises due to uncertain dust corrections of atypical galaxies that dominate the SFR budget; for example, high inclination galaxies (e.g., M 82) or galaxies with large fore-

ground Galactic extinction (e.g., NGC 6946).

3.3. *Total SFR within* 11 *Mpc*

We derive the total SFR within the 11 Mpc volume and compare to the cosmic SFR density. For this we must assume a local overdensity factor. For example, at distances of 1–5 Mpc, Drozdovsky et al. (2008) demonstrates more than factor 2 overdensity over the cosmic SFR. Karachentsev et al. (2004) studied the B-band luminosity density of the local 8 Mpc and found it to be 1.7–2.0 times the global luminosity density as measured by the SDSS and the Millennium Galaxy Catalogue. Using an overdensity factor of 1.7, and adjusting to the NOROT calibration, the $z = 0$ extrapolation of the HB06 best-fit cosmic SFR density predicts a total SFR within 11 Mpc of $220^{+40}_{-30}\,\mathrm{M_\odot yr^{-1}}$. Similarly, the ROT calibration yields $170^{+30}_{-30}\,\mathrm{M_\odot yr^{-1}}$. In both estimates we use the UV calibration, since the HB06 compilation in the redshift range $0 < z < 1$ is dominantly based on the UV indicator.

We directly estimate the total SFR within 11 Mpc by starting with the 11HUGS + $GALEX$ galaxy catalog and applying the same two-tier Galactic latitude cut as is used in the LVL survey, namely, $|b| \geq 20^\circ$ for distances < 3.5 Mpc and $|b| \geq 30^\circ$ for distances of 3.5 to 11 Mpc. This leaves a sample of 282 galaxies with positive Hα and FUV flux measurements. The fraction of the 11 Mpc sphere included after these cuts is $\sim 51\%$, and we estimate the total SFR by summing the SFR of the galaxies and dividing by the volume fraction.

The Hα luminosities are corrected for the [NII] line contamination, underlying stellar absorption, and Galactic foreground extinction following Kennicutt et al. (2008). We correct for internal attenuation using the empirical scaling correction with the host galaxy B-band magnitude (Lee et al. 2009) of

$$A_{H\alpha} = \begin{cases} 0.10 & M_B > -14.5 \\ 1.971 + 0.323 M_B + 0.0134 M_B^2 & M_B \leq -14.5 \end{cases} \quad (2)$$

For the FUV measurements, we correct for internal attenuation based on the tight correlation with the TIR/FUV ratio (Burgarella et al. 2005),

$$A(\mathrm{FUV}) = -0.028x^3 + 0.392x^2 + 1.094x + 0.546, \quad (3)$$

applicable for galaxies with recent star formation such as the spirals and irregulars. Here, $x = \log[L(\mathrm{TIR})/L(\mathrm{FUV})_{\mathrm{obs}}]$. When the TIR data gives a negative correction, or when TIR data is not available, we use the empirical relation $A(\mathrm{FUV}) = 1.8A(\mathrm{H}\alpha)$ of Lee et al. (2009). These corrections are similar to those applied in previous studies (Lee et al. 2009; Botticella et al. 2012). Finally, we modify the UV calibrations of Table 1 to reflect the central wavelength of the $GALEX$ FUV filter, 0.1532μm. For the NOROT, we find that

$$\log \mathrm{SFR}\,[\mathrm{M_\odot yr^{-1}}] = \log(\mathrm{L_{FUV,corr}[L_\odot]}) - 9.51, \quad (4)$$

which is very similar to the $GALEX$ calibration reported in Iglesias-Páramo et al. (2006) who uses the Starburst99 synthesis code (Leitherer et al. 1999) with the solar metallicity Geneva non-rotating tracks and a Salpeter IMF from 0.1–$100 M_\odot$.

TABLE 2
SUMMARY OF TOTAL SFR ESTIMATES WITHIN 11 MPC

	SFR ($M_\odot$ yr^{-1})
Cosmic extrapolation (NOROT)	220 ± 40
Direct Hα (NOROT)	120 ± 20
Direct UV (NOROT)	170 ± 20
Cosmic extrapolation (ROT)	170 ± 30
Direct Hα (ROT)	80 ± 10
Direct UV (ROT)	130 ± 20
CCSN with 08S-like objects	360^{+120}_{-90}
CCSN without 08S-like objects	270^{+110}_{-80}

NOTE. — These are the total SFR, i.e., sky-coverage corrected where appropriate (see text). All for a Salpeter IMF. The cosmic extrapolation is corrected for the local overdensity by a factor of 1.7. For CCSNe, a supernova mass range of 8–40 $M_\odot$ is adopted; the upper mass limit is not important (see text).

We summarize our results in Table 2. The direct SFR estimates are generally smaller than the cosmic extrapolations, but the UV-SFR is consistent within the uncertainties. The Hα estimates, on the other hand, fall short of the cosmic extrapolation. One possibility is that we have slightly overestimated the local overdensity, since we adopt an overdensity derived from ~ 8 Mpc scales for the entire 11 Mpc volume.

As mentioned in the previous section, the stochastic nature of star formation can be an issue. Since PEGASE.2 is a deterministic synthesis code, it does not cover the stochastic behavior at low SFR rates. This occurs when the number of massive stars falls below ~ 10. However, we are summing over a sufficient number of galaxies with a sufficiently large total SFR that the stochasticity is not a problem. More quantitatively, the Hα indicator is related to stars with $M \gtrsim 20\,M_\odot$. Adopting the Salpeter IMF, $5 \times 10^3\,M_\odot$ of stellar material must be made for there to be 10 such stars, and this must continue at least over the lifetime of the massive stars, some 3 Myr. Thus, the required SFR is at least $\sim 2 \times 10^{-3}\,\mathrm{M_\odot\,yr^{-1}}$ per galaxy. If we adopt more modern IMFs where the number of low mass stars are suppressed relative the Salpeter IMF, there will be more massive stars for a given total stellar mass and the required SFR will only decrease.

4. COMPARISON TO CORE-COLLAPSE SUPERNOVA RATES

The most massive stars in a star formation burst evolve the fastest and then explode as CCSNe. Therefore, observations of CCSNe are excellent proxies of recent star formation that is far less sensitive to modest dust. Different types of CCSNe probe the SFR on different time scales; treated together, CCSNe probe the SFR on time scales similar to the UV indicator. A well-measured CCSN rate yields an estimate of the SFR normalization, and even the observation of a few CCSNe yields lower limits. We use both the cosmic CCSNe and CCSNe in the local volume and discuss how compatible they are with the rotation calibrations.

The CCSN rate, $\dot{N}_{\mathrm{CCSN}}$, is related to the SFR, $\dot{M}_*$, by

TABLE 3
LOCAL CCSNE (IN BOLD, TOTAL 17) AND POSSIBLE CCSNE (IN ITALIC, TOTAL 5) WITHIN 11 MPC DURING 2000 TO 2011 INCLUSIVE

SN	Galaxy	Type	D (Mpc)	R.A.	Decl.	b (deg)	11HUGS Full	11HUGS LVLcut	LVL
SN 2002ap	NGC 0628	IcPec	7.3	01 36 41.7	15 46 59	−45.7	Y	Y	Y
SN 2002bu	NGC 4242	SN?[1]	7.4	12 17 30.1	45 37 08	70.3	Y	Y	Y
SN 2002hh	NGC 6946	IIP	5.9	20 34 52.3	60 09 14	11.7	Y	-	-
SN 2003gd	NGC 0628	IIP	7.3	01 36 41.7	15 46 59	−45.7	Y	Y	Y
SN 2004am	NGC 3034 (M 82)	IIP	3.5	09 55 52.2	69 40 47	40.6	Y	Y	Y
SN 2004dj	NGC 2403	IIP	3.2	07 36 51.4	65 36 09	29.2	Y	Y	Y
SN 2004et	NGC 6946	IIP	5.9	20 34 52.3	60 09 14	11.7	Y	-	-
SN 2005af	NGC 4945	IIP	3.6	13 05 27.5	−49 28 06	13.3	Y	-	-
SN 2005at	NGC 6744	Ic	9.4	19 09 46.2	−63 51 25	−26.1	Y	-	-
SN 2005cs	NGC 5194 (M 51)	IIP	8.0	13 29 52.7	47 11 43	68.6	Y	Y	Y
SN 2007gr	NGC 1058	Ic	9.2	02 43 29.9	37 20 27	−20.4	Y	-	-
SN 2008S	NGC 6946	SN?[2]	5.9	20 34 52.3	60 09 14	11.7	Y	-	-
SN 2008ax	NGC 4490	IIb	8.0	12 30 36.1	41 38 34	74.9	Y	Y	Y
SN 2008bk	NGC 7793	IIP	3.9	23 57 49.7	−32 35 30	−77.2	Y	Y	Y
NGC300-OT	NGC 0300	SN?[3]	2.0	00 54 53.5	−37 41 00	−79.4	Y	Y	-
SN 2008iz	NGC 3034 (M 82)	II	3.5	09 55 52.2	69 40 47	40.6	Y	Y	Y
SN 2008jb	ESO 302-14	IIP	9.6	03 51 40.9	−38 27 08	−50.9	Y	Y	-
SN 2009hd	NGC 3627 (M 66)	IIP	10.1	11 20 15.0	12 59 30	64.4	Y	Y	Y
SN 2010da	NGC 0300	SN?[4]	2.0	00 54 53.5	−37 41 00	−79.4	Y	Y	-
SN 2011dh	NGC 5194 (M 51)	IIb	8.0	13 29 52.7	47 11 43	68.6	Y	Y	Y
PSN J12304185+4137498	NGC 4490	SN?[5]	8.0	12 30 36.1	41 38 34	74.9	Y	Y	Y
SN 2011ja	NGC 4945	IIP	3.6	13 05 27.5	−49 28 06	13.3	Y	-	-

NOTE. — [1]Thompson et al. (2009); Smith et al. (2011); Szczygieł et al. (2012b), [2]Prieto et al. (2008, 2009); Smith et al. (2009); Botticella et al. (2009); Pumo et al. (2009); Prieto et al. (2010); Szczygieł et al. (2012a), [3]Bond et al. (2009); Berger et al. (2009); Prieto et al. (2009); Kashi et al. (2010); Kochanek et al. (2012), [4]Elias-Rosa et al. (2010), [5]Cortini et al. (2011); Fraser et al. (2011); Magill et al. (2011)

$\dot{N}_{\rm CCSN} = \dot{M}_*/f_{\rm CCSN}$, where $f_{\rm CCSN}$ is calculated as

$$f_{\rm CCSN} = \frac{\int_{0.1}^{100} M\psi(M)dM}{\int_{M_{\rm min}}^{M_{\rm max}} \psi(M)dM}, \quad (5)$$

where $0.1M_\odot$ and $100M_\odot$ in the numerator is the range of the IMF, and $M_{\rm min}$ to $M_{\rm max}$ in the denominator is the mass range of stars that explode as CCSNe. Note that Eq. (5) is the inverse of the CCSN efficiency. Due to the steep IMF slope, the majority of CCSNe occur near the minimum mass threshold, making $M_{\rm min}$ the most important parameter. Its value has been statistically determined by combining 20 Type IIP supernova progenitor observations to be $M_{\rm min}^{\rm IIP} = 8.5^{+1}_{-1.5}M_\odot$ (Smartt et al. 2009). This is consistent with the highest masses estimated for white dwarf progenitors, $\sim 7\,{\rm M}_\odot$ (Williams et al. 2009). Thus, two different approaches seem to be converging to $M_{\rm min} \approx 8 \pm 1\,{\rm M}_\odot$. As we show below, this uncertainty affects $f_{\rm CCSN}$ by $\sim 20\%$.

The value of $M_{\rm max}$ is more uncertain than $M_{\rm min}$, but is less important. The maximum mass from Type IIP supernova progenitors is found to be $M_{\rm max}^{\rm IIP} = 16.5 \pm 1.5\,M_\odot$ (Smartt et al. 2009), but consideration of other types of SNe—including Types IIn and Ibc—yields larger values. For example, it is widely expected that Type Ibc SNe originate from evolved massive stars that have shed their envelopes, whose initial masses are $\gtrsim 25\,M_\odot$. The spatial distribution of CCSNe supports that Type Ibc progenitors must be more massive than those of Type IIP SNe (Anderson & James 2008, 2009). Theoretically, stars with masses above $M_{\rm max} \sim 40\,M_\odot$ may promptly form black holes whose optical transient phenomena remains uncertain (e.g., Fryer 1999; Kochanek et al. 2008). We adopt $M_{\rm max} = 40\,M_\odot$ as our canonical value, which together with $M_{\rm min} = 8 \pm 1\,M_\odot$ yields $f_{\rm CCSN} = 147^{+27}_{-29}/M_\odot$, a $\sim 20\%$ uncertainty. On the other hand, varying $M_{\rm max}$ between $25M_\odot$ and $100M_\odot$ only affects $f_{\rm CCSN}$ by $\sim 5\%$. We refer the reader to Horiuchi et al. (2011) for detailed discussions of the uncertainties in the SFR-to-CCSN rate connection.

One of the advantages of CCSNe is that the SFR normalization can be probed without significant dependence on the IMF. This is because the mass range of stars exploding as CCSNe is similar to the mass range of stars powering the radiation used to measure the SFR. For example, we can write explicitly the SFR estimated from the UV and CCSNe as $f_{\rm UV}L_{\rm UV}$ and $f_{\rm CCSN}\dot{N}_{\rm CCSN}$. Although changes to the IMF affects $f_{\rm UV}$ and $f_{\rm CCSN}$ individually by factors of ~ 2, their ratio remains fairly constant. For the SalA and BG IMFs, $f_{\rm UV}/f_{\rm CCSN} = 1.09 \times 10^{-30}\,{\rm yr}^{-1}\,{\rm erg}^{-1}\,{\rm s\,Hz}$ and $1.01 \times 10^{-30}\,{\rm yr}^{-1}\,{\rm erg}^{-1}\,{\rm s\,Hz}$, respectively, which are within 10% of the Salpeter IMF value $1.09 \times 10^{-30}\,{\rm yr}^{-1}\,{\rm erg}^{-1}\,{\rm s\,Hz}$.

4.1. *Comparison at cosmic distances*

Measurements of the CCSN rate at cosmic distances have rapidly increased in the past decade. Taking the measurements of Cappellaro et al. (1999); Dahlen et al. (2004); Cappellaro et al. (2005); Botticella et al. (2009); Bazin et al. (2009); Li et al. (2011), the observed CCSN rate is well-fit by a strong redshift evolution of $(1+z)^{3.3}$ between $0 < z < 1$ with a $z = 0$ normalization of $0.72^{+0.2}_{-0.2} \times 10^{-4}\,{\rm Mpc}^{-3}\,{\rm yr}^{-1}$.

By comparison, the CCSN rate predicted from the SFR using the NOROT calibration and Equation (5) has a $z = 0$ normalization that is twice as large, $1.5^{+0.3}_{-0.2} \times 10^{-4}\,\mathrm{Mpc^{-3}\,yr^{-1}}$. Uncertainties associated with calculating the CCSN rate from the SFR seem not to be able to satisfactorily explain the difference (e.g., Hopkins & Beacom 2006; Horiuchi et al. 2011).

Rotation helps bridge the normalization difference by decreasing the SFR and hence the predicted CCSN rate. However, the reduction is expected to be at most $\sim 30\%$, which is not enough to bridge the difference completely. Furthermore, it has been argued that a combination of intrinsically dim and heavily dust-obscured CCSNe being missed in CCSN surveys could be responsible for the observed discrepancy (Horiuchi et al. 2011). Indeed, the most recent direct CCSN rate measurement by Dahlen et al. (2012) takes into account missed dim CCSNe and find the discrepancy with the SFR is substantially reduced, supporting this explanation.

4.2. *Comparison at local distances*

Discoveries of CCSNe in the nearby volume have also improved recently. In Table 3, we show a list of CCSNe discovered within ~ 11 Mpc in the past 12 years from 2000 to 2011 inclusive. Similar compilations can be found in Horiuchi et al. (2011); Botticella et al. (2012); Mattila et al. (2012). We exclude previous years due to known supernova incompleteness issues (Horiuchi & Beacom 2010). Distances are taken from the 11HUGS catalog (Kennicutt et al. 2008). These are estimated from a combination of direct stellar distances (where available) and flow-corrected radial velocities. The Local Group flow model of Karachentsev & Makarov (1996) is used, which the authors find to be more accurate for the 11 Mpc volume than a Virgocentric flow model. The last three columns show whether the host galaxy is included in the respective galaxy catalogs as labeled.

Included in Table 3 are SN 2008S-like events (SN 2008S, SN 2002bu, NGC300-OT, SN 2010da, and PSN J12304185+4137498) whose true nature continues to be debated. They are characterized by explosions that are 2–3 mag dimmer than regular CCSNe, with narrow emission lines, and evidence of internal extinction; their progenitors are also dust enshrouded (Prieto et al. 2008). While they are relatively common among nearby CCSNe, their progenitors are extremely rare (Khan et al. 2010), leading Thompson et al. (2009) to propose that many massive stars go through this dust-obscured phase shortly ($\sim 10^4$ yr) before the explosion. SN 2008S-like events may be true CCSNe, perhaps of the electron-capture type arising from asymptotic giant branch stars (Thompson et al. 2009; Botticella et al. 2009; Pumo et al. 2009), or they may be extreme versions of non-explosive outbursts (Thompson et al. 2009; Smith et al. 2009; Bond et al. 2009; Berger et al. 2009; Kashi et al. 2010; Smith et al. 2011). For a comprehensive discussion of these and related models, see, e.g., Thompson et al. (2009); Smith et al. (2011); Kochanek (2011); Kochanek et al. (2012).

The compilation is a lower limit of the true CCSNe occurrence. This is because the CCSN discoveries are mainly made by surveys and amateurs with varying search strategies and methods, instead of a complete systematic survey. Although modern telescopes using CCDs are capable of discovering a typical CCSN within 11 Mpc, CCSNe can be missed due to a combination of incomplete galaxy coverage, low survey cadence, heavily dust-obscured or dim CCSNe, or obstruction by the Galactic plane and the Sun. Indeed, the majority of CCSNe have occurred in large, well-known galaxies: all 22 CCSNe occurred in the full 11HUGS galaxy catalog. Also, 15 of these occurred in our galaxy sample with LVL cuts. Since the LVL sky-coverage is only 51%, we are likely missing some CCSNe occurring in the remaining volume. Furthermore, the northern hemisphere is more closely observed, resulting in somewhat more CCSNe discovered with positive declinations than with negative declinations (14 versus 8). As a specific example illustrating these points, SN 2008jb remained undiscovered by all galaxy-targeted supernova searches despite its close distance of 9.6 Mpc. The host galaxy was a dwarf galaxy in the southern hemisphere, and the CCSN was only discovered in archival images of all-sky surveys (Prieto et al. 2012).

There are 17 definite CCSNe and 5 SN 2008S-like events in Table 3. With our LVL sky-coverage cuts, this is reduced to 11 definite CCSNe and 4 SN 2008S-like events. From Poisson statistics, the 1σ lower and upper limits of the 11 definite CCSNe are 7.7 and 15.4, which gives a CCSN rate of $1.8^{+0.7}_{-0.5}\,\mathrm{yr^{-1}}$ within the 11 Mpc volume, where we have applied a sky-coverage correction analogous to the local SFR calculations. The SFR required is simply the CCSN rate multiplied by f_{CCSN}. For our canonical f_{CCSN}, this gives $270^{+110}_{-80}\,\mathrm{M_\odot\,yr^{-1}}$. Repeating the exercise including SN 2008S-like events gives a CCSN rate of $2.5^{+0.8}_{-0.6}\,\mathrm{yr^{-1}}$ and a required SFR of $360^{+120}_{-90}\,\mathrm{M_\odot\,yr^{-1}}$.

The SFR values are summarized in Table 2. The SFR required by CCSNe is consistent given uncertainties with the cosmic SFR extrapolation and the non-rotating UV-SFR, but does not overlap within the uncertainties with all other SFR estimates. However, the uncertainties are large because of uncertain dust corrections on the SFR. If SN 2008S-like events are included, there is an even stronger tension including with the non-rotating UV-SFR. The Hα-SFR show a more significant tension than the UV, but as we have discussed, the CCSN rate probes SFR on time scales that are longer than the Hα indicator and more comparable to the UV.

These SFR values required by CCSNe can be reduced by adopting a larger mass range for CCSNe. However, even with extreme values of $M_{\mathrm{min}} = 7M_\odot$ and $M_{\mathrm{max}} = 100M_\odot$, the required SFR is about $200\,\mathrm{M_\odot\,yr^{-1}}$ ($280\,\mathrm{M_\odot\,yr^{-1}}$) excluding (including) SN 2008S-like events. One possible solution is to further decrease the minimum mass for CCSN. This was studied by Botticella et al. (2012), who suggested the CCSNe and non-rotating Hα-SFR are consistent if $M_{\mathrm{min}} = 6M_\odot$. Although a similarly small M_{min} would be compatible with the rotating predictions, we do not favor this scenario because M_{min} has been accurately determined using progenitor observations of CCSNe in the nearby ~ 20 Mpc volume, i.e., a similar volume (Smartt et al. 2009).

In Figure 5, we show the build up (cumulative) CC-

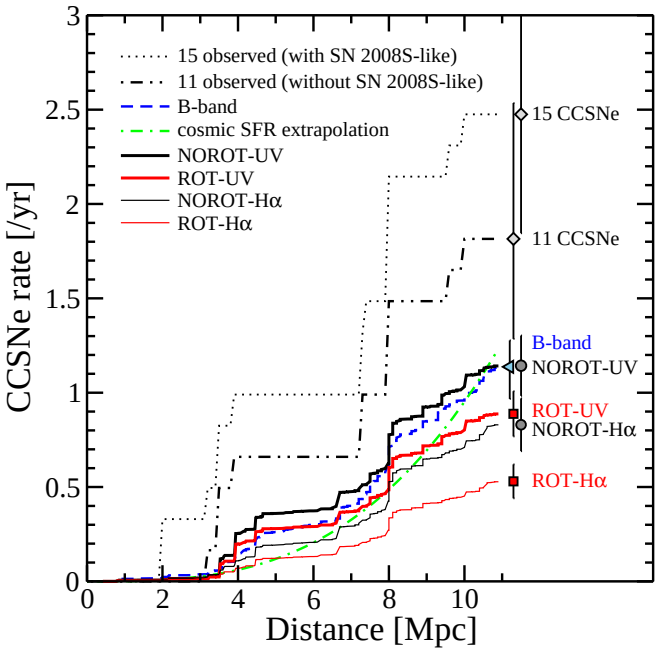

FIG. 5.— The build up of CCSNe (i.e., cumulative), showing the discovered CCSNe with (dotted) and without (dot-dot-dashed) SN 2008S-like events, predictions from the SFR for Hα (thin solid) and UV (thick solid) for non-rotating (black) and rotating (red) calibrations, and prediction based on the B-band (dashed), as labeled. All discoveries and predictions have been subject to the LVL angular cuts and corrected upwards for the missing volume (see text). The total and uncertainty within 11 Mpc are shown by the data point with error bars on the right hand side. There are more CCSNe discovered than predicted, in particular if the rotating calibration is assumed.

SNe as a function of distance, and the value within 11 Mpc as data points. We show the observed CCSNe with and without SN 2008S-like events, and predictions based on the various SFR estimates, as labeled. We also show another CCSN rate estimate based on the galaxy absolute B-band luminosities using the latest SNu ($1\,\mathrm{SNu} = 1\,\mathrm{CCSN}\,/10^{10}L_{\odot,B}\,/\mathrm{century}$) of LOSS (Li et al. 2011). The SNu depends on the galaxy type as well as the galaxy B-band magnitude. The latter is the rate-size relation found by the LOSS group, which introduces a weighting such that smaller galaxies have higher SNu (the LOSS rates without the rate-size relation are in good agreement with previous estimates by Cappellaro et al. 1999). We use the same galaxy sample as we did for the SFR calculation. We correct the galaxy B-band luminosity for foreground Galactic extinction but not for host extinction, since the LOSS SNu have not been corrected for host extinction either. We then sum the CCSN rate from individual galaxies and apply a sky-coverage correction similarly to our SFR calculation.

From Figure 5, it is clear that more CCSNe are discovered than predicted. Of the SFR estimates, only the non-rotating UV-SFR is marginally compatible with the observed CCSNe without SN 2008S-like events. Also, Figure 5 shows that the UV-SFR and B-band predictions are quantitatively very similar. If this is interpreted as the robustness of CCSN rate predictions, it leads to the conclusion that there has been a chance occurrence of excess CCSNe around ~ 4 Mpc where the discovered rate first overshoots the predictions. The statistics are low in this range: there are only 4 CCSNe within 4 Mpc. However, comparing this to the B-band prediction of 0.85 CCSNe gives a chance occurrence of 0.9% (for the entire 11HUGS sample, the respective numbers are 6 CCSNe discovered and 1.3 expected, a 0.2% occurrence). So, it implies a somewhat rare occurrence. Also, it should be noted that the cosmic CCSN rate predicted based on the B-band rates is a factor ~ 2 smaller than the cosmic SFR rate. Although the local and cosmic rates cannot be directly compared, it leaves the possibility that the prediction in the local volume based on the B-band is also slightly low.

5. DISCUSSIONS AND SUMMARY

Based on the new non-rotational (NOROT) and rotational (ROT) stellar tracks of Ekström et al. (2012), we used the stellar evolutionary synthesis code PEGASE.2 to derive SFR calibration factors for non-rotating and rotating stellar populations. The ROT population shows significantly *increased* photon output compared to the NOROT population, which leads to a *decrease* in SFR calibration factors of 30% and 40% for the UV and Hα indicators, respectively (Table 1). Compared to the widely-used non-rotating SFR calibrations of Kennicutt (1998), the ROT calibrations are 10% and 40% smaller, respectively. These changes to the calibration factors are comparable to (or larger than) the uncertainty on the best-fit cosmic SFR of HB06 that is 20–30% (1–3σ) at redshifts between $0 < z < 1$. Thus it is evident that systematic effects such as the SFR calibration factors will need to be understood better for future precision SFR estimates.

We compare the SFR estimates to the measured CCSN rates to investigate whether the rotational calibrations fit with data. At cosmic distances, the best-fit cosmic SFR is too high compared to the measured CCSN rate data by a factor ~ 2. Stellar rotation will decrease the cosmic SFR but not enough to bridge the difference completely. Furthermore, a part of the SFR-CCSN normalization discrepancy may be caused by CCSNe that are missed due to a combination of intrinsically dim and heavily dust obscured CCSNe (Mannucci et al. 2007; Horiuchi et al. 2011); this explanation has been supported at least at high z by recent CCSN rate measurements (Dahlen et al. 2012).

At distances of $\sim$ 10 Mpc, several studies have found hints of an excess of CCSNe (e.g., Ando et al. 2005; Kistler et al. 2011; Horiuchi et al. 2011; Kistler et al. 2012), while Botticella et al. (2012) performed an in-depth investigation and found that the UV-SFR is consistent with the observed CCSNe. We make new estimates of the SFR and CCSN rate in the local 11 Mpc volume, update the discovered CCSNe, and by comparing the two, find support of an excess of discovered CCSNe (Figure 5). Consistent with Botticella et al. (2012), we find that the total UV-SFR is marginally consistent with the observed CCSNe within uncertainties. However, upon closer inspection, we find that this requires a chance excess of CCSNe in the 4 Mpc volume which is rather unlikely (a 0.2–0.9% chance probability). The Hα-SFR underpredicts the observed CCSN rate considerably. Stellar rotation, which decreases both the UV- and Hα-SFR estimates, exacerbates the situation and is therefore disfavored by current data in the local volume. We empha-

size that this result is strengthened by the fact that the locally discovered CCSN counts can only increase as surveys probe more complete galaxy lists at greater cadence and sensitivities. The result is also robust to local overdensities, since both the SFR and CCSN rates will be similarly affected.

Thus, there is a dichotomy between the cosmic CCSN rate predicted from the SFR, which overestimates the cosmic CCSN measurements, and the local CCSN rate predicted from the observed SFR, which slightly underpredicts the local CCSN observations. Unless the SFR calibrations systematically change with distance, the emerging picture is that the SFR calibration factors are constrained to be close to or only slightly larger than the currently used values. If it were smaller, it would severely underpredict the local CCSN rate. If it were larger, it would severely overpredict the cosmic CCSN rate. However, it may be slightly larger, because not all massive stars need to explode as optically bright CCSNe, although the fraction of dark collapses is expected to not exceed $\sim 50\%$ (e.g., Kochanek et al. 2008).

More generally, the local CCSNe discoveries set a lower bound on the SFR, and using this fact we disfavor any significant change to the total energy output among massive stars, including, but not limited to, rotation. An example is the impact of binaries. PEGASE.2 treats binarity only for the purposes of determining chemical enrichment by Type Ia supernovae, but in reality binary interactions affect various aspects of stellar evolution, including mixing, mass loss, and surface rotation. The binary fraction of massive stars is known to be at least in the several tens of percent range (e.g., Mason et al. 1998), and a significant fraction of binaries are estimated to be in triple or higher order systems (García & Mermilliod 2001), which can lead to interesting interactions (e.g., Thompson 2011). Recently, Zhang et al. (2012) found that the UV output of stars is increased, leading to a reduction of the SFR calibrations by ~ 0.2 dex when binaries are included. Such changes are also constrained by the observed CCSNe.

Explanations of the CCSN-SFR dichotomy is itself of interest. Generally, effects that affect one distance regime and not the other are required. Given the simple counting and lower limit nature of the locally discovered CCSNe, the most obvious option in the local volume is to increase the SFR. However, increasing the SFR calibrations will necessarily increase the cosmic SFR as well. This leaves galaxy dust correction as the most realistic explanation. Another possibility is that the local galaxy distances are systematically underestimated. Since the SFR scales with the luminosity, and the CCSNe are simple counting, a $\sim 30\%$ systematic increase in the galaxy distances will increase the SFR to match the discovered CCSN counts. For the cosmic situation, the cosmic CCSN rate may be too low. One possibility is that the cosmic CCSN measurements are missing dim CCSNe as explained above. Horiuchi et al. (2011) shows that the fraction of dim CCSNe observed in the local volume is higher than at cosmic distances, and argues that incorporating dim CCSNe increases the cosmic CCSN measurements to match the cosmic SFR. Alternatively, the cosmic luminosity density used to derive many cosmic CCSN rates may be too low, although such a systematic change over a wide redshift range is not independently motivated.

Changes to the SFR will cause other effects not discussed in this paper. For example, they will affect predictions of the stellar mass density (e.g., Madau et al. 1998; Madau & Pozzetti 2000; Chary & Elbaz 2001; Cole et al. 2001). Current predictions based on the HB06 cosmic SFR are higher by a factor ~ 2 than the direct measurements (Hopkins & Beacom 2006), a fact that has been investigated in the context of IMF shape variations and IMF evolution (Wilkins et al. 2008a,b). Rotation decreases the SFR and hence the stellar mass density prediction, but the comparison to data is more complex. This is because the stellar mass measurements are derived using galaxy SED fittings, and thus are also affected by stellar rotation. Since rotation increases the luminosity output of stars, it is likely to reduce the stellar mass density measurements also. Therefore, variations of the IMF may still be needed. However, quantitative predictions are beyond the scope of this paper since it requires calculating longer times including effects of low and intermediate-mass stars. The SFR has also been compared to the extragalactic background light (Horiuchi et al. 2009; Raue & Meyer 2012). However, this is not a strong probe of the SFR calibration variations, because a smaller calibration is effectively canceled by a larger energy output per stellar population.

The main uncertainty of the present study is the small number of CCSNe (between 11 and 22), and the small number of star-forming galaxies (the largest 10 galaxies contribute $\sim 45\%$ of the total SFR within 11 Mpc) that make dust correction uncertain. Performing comparisons at larger distances with more CCSNe and galaxies will dramatically improve the situation since even an increase in factor of 2 in distance would give a factor ~ 8 increase in the rate. Presently running observation programs such as the All-Sky Automated Survey for the Brightest Supernovae (ASAS-SN; e.g., Khan et al. 2011) will find CCSNe in a volume-limited sample of nearby galaxies, and the Palomar Transient Factory will collect larger numbers of CCSNe in survey mode (Law et al. 2009; Lien & Fields 2009). Issues such as completeness should therefore improve dramatically in the near future. Uncertainties inherent to the SFR–CCSN comparison, e.g., the progenitor mass range for CCSN, is rapidly reducing (Smartt 2009). CCSNe will provide an excellent and compelling measure of the SFR in the future that would enable a new way of studying various SFR systematic effects.

We thank Andrew Hopkins, Jennifer Johnson, Rob Kennicutt, Kohta Murase, Marc Pinsonneault, Jose Prieto, and Kris Stanek for useful discussions. We especially thank Christopher Kochanek for discussions and a careful reading of the manuscript. This research made use of the IAU Central Bureau for Astronomical Telegrams and the Sternberg Astronomical Institute supernova catalogs and the NASA/IPAC Extragalactic Database (NED), which is operated by JPL/Caltech, under contract with NASA. This work is supported in part by a JSPS fellowship for research abroad (to SH), and by NSF Grant PHY-1101216 (to JFB).

REFERENCES

Alongi, M., Bertelli, G., Bressan, A., et al. 1993, A&AS, 97, 851
Ando, S., Beacom, J. F., Yüksel, H. 2005, Physical Review Letters, 95, 171101
Althaus, L. G., & Benvenuto, O. G. 1997, ApJ, 477, 313
Anderson, J. P., & James, P. A. 2008, MNRAS, 390, 1527
Anderson, J. P., & James, P. A. 2009, MNRAS, 399, 559
Bazin, G., et al. 2009, A&A, 499, 653
Baldry, I. K., & Glazebrook, K. 2003, ApJ, 593, 258
Bell, E. F., & Kennicutt, R. C., Jr. 2001, ApJ, 548, 681
Bell, E. F. 2003, ApJ, 586, 794
Berger, E., et al. 2009, ApJ, 699, 1850
Bond, H. E., Bedin, L. R., Bonanos, A. Z., Humphreys, R. M., Monard, L. A. G. B., Prieto, J. L., & Walter, F. M. 2009, ApJ, 695, L154
Bothwell, M. S., Kennicutt, R. C., & Lee, J. C. 2009, MNRAS, 400, 154
Bothwell, M. S., Kenicutt, R. C., Johnson, B. D., et al. 2011, MNRAS, 415, 1815
Botticella, M. T., Riello, M., Cappellaro, E., et al. 2008, A&A, 479, 49
Botticella, M. T., et al. 2009, MNRAS, 398, 1041
Botticella, M. T., Smartt, S. J., Kennicutt, R. C., et al. 2012, A&A, 537, A132
Bressan, A., Fagotto, F., Bertelli, G., & Chiosi, C. 1993, A&AS, 100, 647
Brott, I., de Mink, S. E., Cantiello, M., et al. 2011, A&A, 530, A115
Buat, V. 1992, A&A, 264, 444
Buat, V., Donas, J., & Deharveng, J. M. 1987, A&A, 185, 33
Buat, V., Boselli, A., Gavazzi, G., & Bonfanti, C. 2002, A&A, 383, 801
Burgarella, D., Buat, V., & Iglesias-Páramo, J. 2005, MNRAS, 360, 1413
Calzetti, D., Kennicutt, R. C., Engelbracht, C. W., et al. 2007, ApJ, 666, 870
Calzetti, D., Wu, S.-Y., Hong, S., et al. 2010, ApJ, 714, 1256
Cappellaro, E., Evans, R., & Turatto, M. 1999, A&A, 351, 459
Cappellaro, E., et al. 2005, A&A, 430, 83
Chabrier, G., & Baraffe, I. 1997, A&A, 327, 1039
Chary, R., & Elbaz, D. 2001, ApJ, 556, 562
Cole, S., Norberg, P., Baugh, C. M., et al. 2001, MNRAS, 326, 255
Condon, J. J. 1992, ARA&A, 30, 575
Cortini, G., Borkovits, T., Szakats, R., & Brimacombe, J. 2011, Central Bureau Electronic Telegrams, 2789, 1
Dahlen, T., Strolger, L.-G., Riess, A. G., et al. 2004, ApJ, 613, 189
Dahlen, T., Strolger, L.-G., Riess, A. G., et al. 2012, arXiv:1208.0342
Dale, D. A., Cohen, S. A., Johnson, L. C., et al. 2009, ApJ, 703, 517
Drout, M. R., Massey, P., & Meynet, G. 2012, arXiv:1203.0247
Drozdovsky, I., Hopkins, A., Aparicio, A., & Gallart, C. 2008, Galaxies in the Local Volume, 143
Ekström, S., Georgy, C., Eggenberger, P., et al. 2012, A&A, 537, A146
Elias-Rosa, N., Mauerhan, J. C., & van Dyk, S. D. 2010, The Astronomer's Telegram, 2636, 1
Fagotto, F., Bressan, A., Bertelli, G., & Chiosi, C. 1994, A&AS, 104, 365
Fagotto, F., Bressan, A., Bertelli, G., & Chiosi, C. 1994, A&AS, 105, 29
Fagotto, F., Bressan, A., Bertelli, G., & Chiosi, C. 1994, A&AS, 105, 39
Fioc, M., & Rocca-Volmerange, B. 1999, arXiv:astro-ph/9912179
Fraser, M., Kotak, R., Magill, L., Smartt, S. J., & Pastorello, A. 2011, The Astronomer's Telegram, 3574, 1
Fryer, C. L. 1999, ApJ, 522, 413
García, B., & Mermilliod, J. C. 2001, A&A, 368, 122
Georgy, C. 2012, A&A, 538, L8
Georgy, C., Ekström, S., Meynet, G., et al. 2012, arXiv:1203.5243
Gil de Paz, A., Boissier, S., Madore, B. F., et al. 2007, ApJS, 173, 185
Girardi, L., Bressan, A., Chiosi, C., Bertelli, G., & Nasi, E. 1996, A&AS, 117, 113
Groenewegen, M. A. T., & de Jong, T. 1993, A&A, 267, 410
Hanish, D. J., Meurer, G. R., Ferguson, H. C., et al. 2006, ApJ, 649, 150
Heger, A., & Langer, N. 2000, ApJ, 544, 1016
Hopkins, A. M., Connolly, A. J., Haarsma, D. B., & Cram, L. E. 2001, AJ, 122, 288
Hopkins, A. M., Miller, C. J., Nichol, R. C., et al. 2003, ApJ, 599, 971
Hopkins, A. M. 2004, ApJ, 615, 209
Hopkins, A. M., & Beacom, J. F. 2006, ApJ, 651, 142
Horiuchi, S., Beacom, J. F., & Dwek, E. 2009, Phys. Rev. D, 79, 083013
Horiuchi, S., & Beacom, J. F. 2010, ApJ, 723, 329
Horiuchi, S., Beacom, J. F., Kochanek, C. S., et al. 2011, ApJ, 738, 154
Huang, W., Gies, D. R., & McSwain, M. V. 2010, ApJ, 722, 605
Iglesias-Páramo, J., Boselli, A., Gavazzi, G., & Zaccardo, A. 2004, A&A, 421, 887
Iglesias-Páramo, J., Buat, V., Takeuchi, T. T., et al. 2006, ApJS, 164, 38
Karachentsev, I. D., & Makarov, D. A. 1996, AJ, 111, 794
Karachentsev, I. D., Karachentseva, V. E., Huchtmeier, W. K., & Makarov, D. I. 2004, AJ, 127, 2031
Kashi, A., Frankowski, A., & Soker, N. 2010, ApJ, 709, L11
Kennicutt, R. C., Jr. 1992, ApJ, 388, 310
Kennicutt, R. C., Jr. 1998, ARA&A, 36, 189
Kennicutt, R. C., Jr., Lee, J. C., Funes, S. J., José G., Sakai, S., & Akiyama, S. 2008, ApJS, 178, 247
Kennicutt, R. C., Jr., Hao, C.-N., Calzetti, D., et al. 2009, ApJ, 703, 1672
Khan, R., Stanek, K. Z., Prieto, J. L., et al. 2010, ApJ, 715, 1094
Khan, R., Prieto, J. L., Pojmański, G., et al. 2011, ApJ, 726, 106
Kistler, M. D., Yüksel, H., Ando, S., Beacom, J. F., & Suzuki, Y. 2011, Phys. Rev. D, 83, 123008
Kistler, M. D., Haxton, W. C.,Yüksel, H. 2012, arXiv:1211.6770
Kobayashi, M. A. R., Inoue, Y., & Inoue, A. K. 2012, arXiv:1208.0489
Kochanek, C. S., Beacom, J. F., Kistler, M. D., et al. 2008, ApJ, 684, 1336
Kochanek, C. S., Szczygiel, D. M., & Stanek, K. Z. 2011, ApJ, 737, 76
Kochanek, C. S. 2011, ApJ, 741, 37
Kochanek, C. S., Szczygieł, D. M., & Stanek, K. Z. 2012, ApJ, 758, 142
Kroupa, P. 2001, MNRAS, 322, 231
Kudritzki, R. P., Pauldrach, A., Puls, J., & Abbott, D. C. 1989, A&A, 219, 205
Langer, N. 2012, ARA&A, 50, 107
Law, N. M., et al. 2009, PASP, 121, 1395
Lejeune, T., & Schaerer, D. 2001, A&A, 366, 538
Lee, J. C., Gil de Paz, A., Tremonti, C., et al. 2009, ApJ, 706, 599
Lee, J. C., Gil de Paz, A., Kennicutt, R. C., Jr., et al. 2011, ApJS, 192, 6
Leitherer, C., Schaerer, D., Goldader, J. D., et al. 1999, ApJS, 123, 3
Leitherer, C. 2008, IAU Symposium, 255, 305
Leitherer, C., & Ekstrom, S. 2011, arXiv:1111.5204
Levesque, E. M., Leitherer, C., Ekstrom, S., Meynet, G., & Schaerer, D. 2012, ApJ, 751, 67
Li, W., Chornock, R., Leaman, J., et al. 2011, MNRAS, 412, 1473
Lien, A., & Fields, B. D. 2009, JCAP, 1, 47
Lilly, S. J., Le Fevre, O., Hammer, F., & Crampton, D. 1996, ApJ, 460, L1
Lonsdale Persson, C. J., & Helou, G. 1987, ApJ, 314, 513
Madau, P., Ferguson, H. C., Dickinson, M. E., et al. 1996, MNRAS, 283, 1388
Madau, P., Pozzetti, L., & Dickinson, M. 1998, ApJ, 498, 106
Madau, P., & Pozzetti, L. 2000, MNRAS, 312, L9
Maeder, A., & Meynet, G. 2000, ARA&A, 38, 143
Magill, L., Kotak, R., Fraser, M., et al. 2011, Central Bureau Electronic Telegrams, 2789, 2
Mannucci, F., Della Valle, M., & Panagia, N. 2007, MNRAS, 377, 1229
Mason, B. D., Gies, D. R., Hartkopf, W. I., et al. 1998, AJ, 115, 821
Mattila, S., Dahlen, T., Efstathiou, A., et al. 2012, ApJ, 756, 111
Meurer, G. R., Wong, O. I., Kim, J. H., et al. 2009, ApJ, 695, 765
Meynet, G., & Maeder, A. 2000, A&A, 361, 101
Moustakas, J., Kennicutt, R. C., Jr., & Tremonti, C. A. 2006, ApJ, 642, 775
Neugent, K. F., Massey, P., Skiff, B., & Meynet, G. 2012, ApJ, 749, 177
Prieto, J. L., Kistler, M. D., Thompson, T. A., et al. 2008, ApJ, 681, L9
Prieto, J. L., Sellgren, K., Thompson, T. A., & Kochanek, C. S. 2009, ApJ, 705, 1425
Prieto, J. L., Szczygiel, D. M., Kochanek, C. S., et al. 2010, arXiv:1007.0011
Prieto, J. L., Lee, J. C., Drake, A. J., et al. 2012, ApJ, 745, 70
Pumo, M. L., Turatto, M., Botticella, M. T., et al. 2009, ApJ, 705, L138
Raue, M., & Meyer, M. 2012, MNRAS, 426, 1097
Rieke, G. H., Alonso-Herrero, A., Weiner, B. J., et al. 2009, ApJ, 692, 556
Salim, S., Charlot, S., Rich, R. M., et al. 2005, ApJ, 619, L39
Salim, S., Rich, R. M., Charlot, S., et al. 2007, ApJS, 173, 267
Salpeter, E. E. 1955, ApJ, 121, 161
Sauvage, M., & Thuan, T. X. 1992, ApJ, 396, L69
Schaller, G., Schaerer, D., Meynet, G., & Maeder, A. 1992, A&AS, 96, 269
Smartt, S. J., Eldridge, J. J., Crockett, R. M., & Maund, J. R. 2009, MNRAS, 395, 1409
Smartt, S. J. 2009, ARA&A, 47, 63
Smith, N., Ganeshalingam, M., Chornock, R., et al. 2009, ApJ, 697, L49
Smith, N., Li, W., Silverman, J. M., Ganeshalingam, M., & Filippenko, A. V. 2011, MNRAS, 415, 773
Steidel, C. C., Adelberger, K. L., Giavalisco, M., Dickinson, M., & Pettini, M. 1999, ApJ, 519, 1
Szczygieł, D. M., Prieto, J. L., Kochanek, C. S., et al. 2012a, ApJ, 750, 77
Szczygieł, D. M., Kochanek, C. S., & Dai, X. 2012b, ApJ, 760, 20
Thompson, T. A., Prieto, J. L., Stanek, K. Z., et al. 2009, ApJ, 705, 1364
Thompson, T. A. 2011, ApJ, 741, 82
Wilkins, S. M., Trentham, N., & Hopkins, A. M. 2008a, MNRAS, 385, 687

Wilkins, S. M., Hopkins, A. M., Trentham, N., & Tojeiro, R. 2008b, MNRAS, 391, 363
Williams, K. A., Bolte, M., & Koester, D. 2009, ApJ, 693, 355
Woosley, S. E., & Weaver, T. A. 1995, ApJS, 101, 181
Zhang, F., Li, L., Zhang, Y., Kang, X., & Han, Z. 2012, MNRAS, 421, 743